Supplement of Atmos. Chem. Phys., 24, 2099–2112, 2024
https://doi.org/10.5194/acp-24-2099-2024-supplement

Atmospheric Chemistry and Physics
Open Access
EGU

Supplement of

Oxygenated organic molecules produced by low-NO_x photooxidation of aromatic compounds: contributions to secondary organic aerosol and steric hindrance

Xi Cheng et al.

Correspondence to: Yong Jie Li (yongjieli@um.edu.mo) and Qi Chen (qichenpku@pku.edu.cn)

S1. Methods

Loss rate of OOMs

Losses of oxygenated organic molecules (OOMs) in an oxidation flow reactor (OFR) include the loss to the OFR walls (k_{wall}, s^{-1}), the loss to non-condensable products due to continuous reaction with OH (k_{OHloss}, s^{-1}), and the loss to aerosol particles presented in the OFR (i.e., the condensation sink, CS, s^{-1}). These three loss rates are combined to determine the loss rate of OOMs (k_{loss}, s^{-1}), $k_{loss} = k_{wall} + k_{OHloss} + CS$ (Palm et al., 2016).

According to McMurry and Grosjean (1985), $k_{wall} = \frac{A}{V} \cdot \frac{2}{\pi} \cdot \sqrt{k_e D_g}$, where A/V is the OFR surface-area-to-volume ratio (25 m^{-1}), k_e is the coefficient of eddy diffusion (0.0042 s^{-1}) (Huang et al., 2018; Brune, 2019), and D_g is the molecular diffusion coefficient which is determined by the average molecular weight and diffusion volume of OOMs (Kulmala et al., 1998). The average molecular weight and diffusion volume of OOMs varied under different OH exposure, which were calculated on the basis of average OOM formulas. Specifically, the diffusion volume of OOMs was estimated by applying atomic (carbon, hydrogen and oxygen atom numbers) and structural diffusion volume increments (Fuller et al., 1966). The resulted D_g was 0.05 -0.07 $cm^2\ s^{-1}$. The calculated k_{wall} ranged from 0.0023 to 0.0028 s^{-1}. These contributions are minor to k_{loss}. Model also showed a relatively low sensitivity to k_e and D_g over several orders of magnitude (Palm et al., 2016).

The k_{OHloss} were calculated as $k_{OHloss} = \frac{1}{\tau_{OHloss}}$, $\tau_{OHloss} = \frac{5}{k_{OH}[OH]}$. Here, we followed the assumption used in Palm et al. (2016) (1) all OOMs including ROOR' may react with OH for up to five generations, (2) the rate constant for reaction with OH (k_{OH}) is $1.0\times10^{-11}\ cm^3\ molecule^{-1}\ s^{-1}$. The calculated k_{OHloss} is 0.003-0.06 s^{-1}. Palm et al. (2016) showed insensitive OOM fates to k_{OH} and the number of reactions with OH, specifically for values of k_{OH} less than $3\times10^{-11}\ cm^3\ molecule^{-1}\ s^{-1}$ or when assuming 2+ reactions with OH(Palm et al., 2016).

As described by Kulmala et al. (2012), $CS = 4\pi D_g \int_0^\infty r\,\beta(r)N(r)dr$, where r is the radius of particle size bins, $N(r)$ is the particle number size distribution, and $\beta(r)$ is the correction factor for the transition regime. The calculate CS ranged from 0.02 to 0.10 s^{-1}, condensation is an important fate of OOMs for our experiments.

VBS parametrization

The volatility of gaseous OOMs was estimated using volatility parameterization methods. The saturation concentrations (C^*) at 300 K for individual organic compounds are given by Donahue et al. (2011) as follows::

$$\log_{10}C^* = (n_0 - n_C) \times b_C - n_O \times b_O - 2\left(\frac{n_C \times n_O}{n_C + n_O}\right) \times b_{CO} \quad \text{(S1)}$$

Wang et al. (2020) identified that oxygenated products derived from toluene and naphthalene possessed more hydroxyl (-OH) and carboxylic (=O) groups instead of hydroperoxide (-OOH) groups, their experimental saturation concentrations matched well with the estimated ones by using the method of Donahue et al. (2011). In this study, for OOMs composed of carbon, hydrogen, and oxygen atoms, we used equation S1 to estimate volatilities, where $n_0 = 25$, $b_C = 0.475$, $b_O = 2.3$, $b_{CO} = -0.3$, n_C and n_O are the number of carbon and oxygen atoms in the compound, respectively.

The saturation concentrations of compounds at ambient temperature T can be approximated as (Epstein et al., 2010; Donahue et al., 2011):

$$\log_{10}C^*(T) = \log_{10}C^*(300K) + \frac{\Delta H_{vap}}{R\ln(10)}\left(\frac{1}{300} - \frac{1}{T}\right) \quad \text{(S2)}$$

where the evaporation enthalpy ΔH_{vap} was linked to saturation concentration $\log_{10}C^*(300K)$ via:

$$\Delta H_{vap}\ [\text{kJ mol}^{-1}] = -5.7\log_{10}C^*(300K) + 129 \quad \text{(S3)}$$

The OOMs were then grouped into different bins within a volatility basis set (VBS) based on C^* (Donahue et al., 2006), and further classified as follows: ultralow volatility organic compound (ULVOC, $\log C^* \leq -9.5$); extremely low volatility organic compound (ELVOC, $-9.5 < \log C^* \leq -4.5$); low volatility organic compound (LVOC, $-4.5 < \log C^* \leq -0.5$); semi-volatile organic compound (SVOC, $-0.5 < \log C^* \leq 2.5$); intermediate volatility organic compound (IVOC, $2.5 < \log C^* \leq 6.5$) (Shrivastava et al., 2017; Bianchi et al., 2019; Schervish and Donahue, 2020).

Condensation estimation

To evaluate the contribution of OOMs to secondary organic aerosols (SOA) through condensation, we calculated the net condensation flux of the observed OOMs as follows (Tröstl et al., 2016):

$$\phi_p = N_p \times \sigma_p \times s_p \times F_p \quad \text{(S4)}$$

with N_p the particle number concentration, σ_p the particle-vapour collision cross-section, and s_p the deposition rate of vapors at the surface. Combining these three terms to derive the condensation sink (s^{-1}), we obtained the actual time constant for interaction of vapors with particles. The driving force of condensation F_p ($\mu g\ m^{-3}$) was expressed as:

$$F_p = C^v - X_p \Upsilon_p K_p C^* \quad \text{(S5)}$$

where C^v is the vapor (OOMs) concentration, C^* is the saturation concentration, X_p is the mass fraction of OOMs of each VBS bin in the condensed phase, and Υ_p is the mass-based activity coefficient in the condensed phase (assuming $\Upsilon_p = 1$ as in ideal organic solution). The Kelvin term, $K_p = \exp(\frac{4\sigma M}{RT\rho D_p})$, is related to the surface tension σ, molar weight M, and density ρ. Here, an assumed constant density of 1400 kg m^{-3} and a surface tension of 0.03 N m^{-1} were applied for the particles.

When the organic vapors in the gas and condensed phases reach equilibrium (F_p is zero), equilibrium partitioning theory was used to describe the condensation and evaporation of the organics onto or from particle surface (Pankow, 1994). The fraction of species *i* in the condensed phase was defined as:

$$f_i = \frac{1}{1 + C^*/C_{OA}} \quad \text{(S6)}$$

where C_{OA} is the concentration of organic aerosol in the condensed phase.

S2. General mechanism of OH-initiated chemistry of aromatic VOCs

The OH-initiated chemistry of aromatic volatile organic compounds (VOCs) mainly proceeds via addition to the aromatic ring to generate OH-aromatic adducts. If there are alkyl substitutions on the aromatic rings, reactions can also proceed via H-atom abstraction for normally ≤10% probability (Jenkin et al., 2003). The alkyl radicals (R) formed either way react with O_2 and form a variety of RO_2 radicals, which undergo the following reaction channels under low-NO_x conditions: (1) bimolecular reaction route (reacting with HO_2 or RO_2 radicals) to form termination products or alkoxy radicals (RO), (2) phenolic route through HO_2 elimination, and (3) bicyclic intermediate route through cyclization (Jenkin et al., 2003; Nishino et al., 2012). The new alkyl (R) radical from the important pathway (3) can be converted to a new RO_2 radical by incorporating an O_2 molecule, forming a host of monomeric and dimeric OOMs via reactions R-S1 to R-S7 (Cheng et al., 2021; Garmash et al.,

2020). Among these reactions, R-S1 is the autoxidation pathway that incorporates more and more oxygen atoms into the products while forming peroxide groups (-OOH) by internal H-shift; R-S2, R-S3, and R-S5 are termination reactions that lead to various monomeric products with different functional groups; R-S4 and R-S6 are the RO pathway between reactions of RO_2 and HO_2 or RO_2, and subsequent isomerization of RO might result in a new RO_2; R-S7 is the accretion reaction that leads to dimer formation.

Autoxidation pathway:

$$RO_2 \rightarrow \bullet QOOH;\ \bullet QOOH + O_2 \rightarrow R(OOH)O_2 \quad \text{(R-S1)}$$

General RO_2 pathways:

$$RO_2 + HO_2 \rightarrow ROOH + O_2 \text{ (hydroperoxide channel)} \quad \text{(R-S2)}$$

$$RO_2 + HO_2 \rightarrow ROH + O_3 \text{ (hydroxyl channel)} \quad \text{(R-S3)}$$

$$RO_2 + HO_2 \rightarrow RO + OH + O_2 \text{ (alkoxy radical channel)} \quad \text{(R-S4)}$$

$$RO_2 + R'O_2 \rightarrow ROH + R'HC{=}O + O_2 \text{ (hydroxyl/carbonyl channel)} \quad \text{(R-S5)}$$

$$RO_2 + R'O_2 \rightarrow RO + R'O + O_2 \text{ (alkoxy radical channel)} \quad \text{(R-S6)}$$

$$RO_2 + R'O_2 \rightarrow ROOR' + O_2 \text{ (dimer channel)} \quad \text{(R-S7)}$$

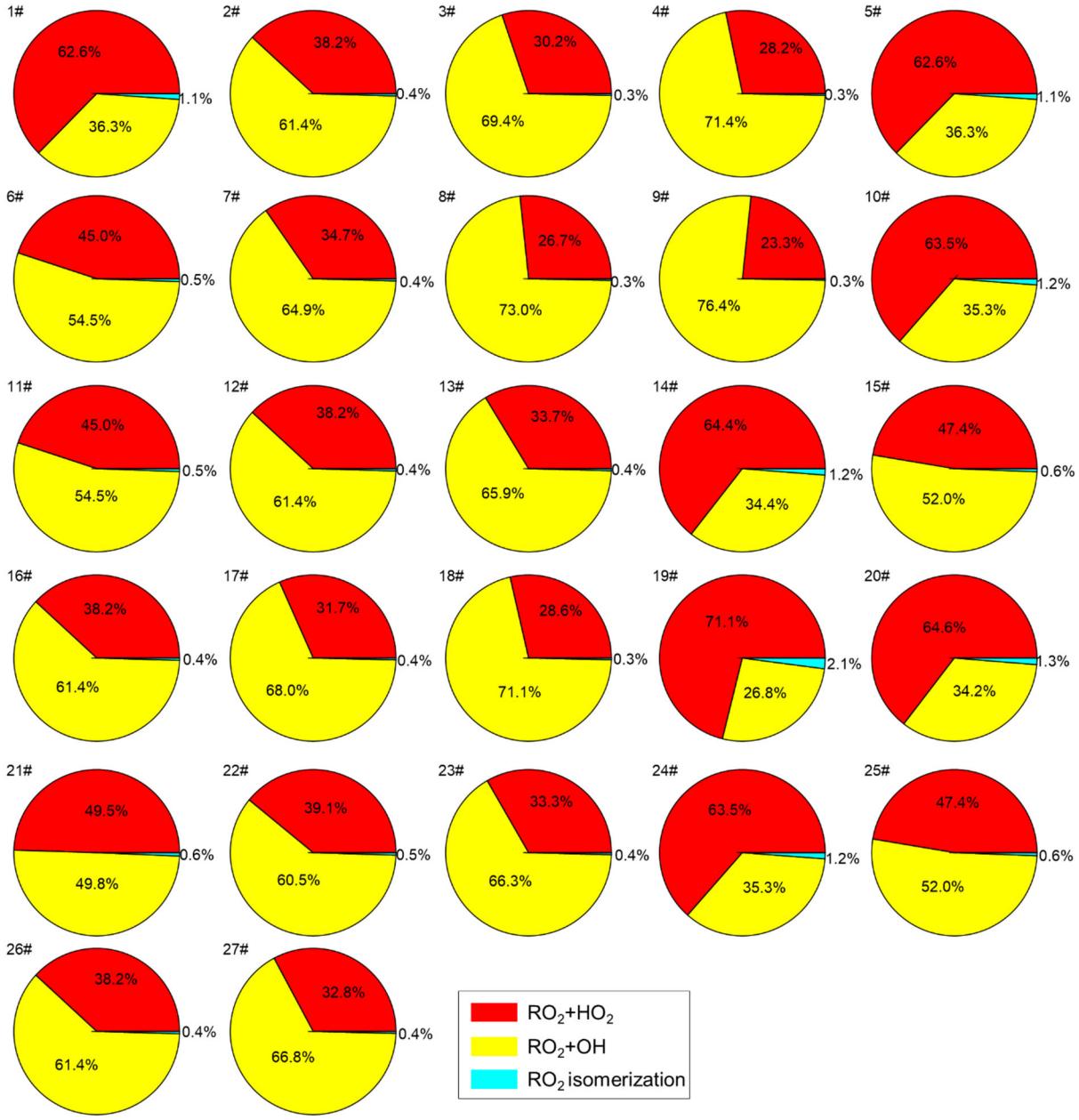

Figure S1. The relative contributions of RO_2 loss channels to the RO_2 fate calculated by using the RO_2 fate estimator (https://sites.google.com/site/pamwiki/estimation-equations) with the measured RO_2 concentrations, the PAMchem-model-derived OH and HO_2 concentrations, and the rate constants of 1.5×10^{-11} cm^3 $molecules^{-1}$ s^{-1} for $RO_2 + HO_2$, 1.0×10^{-10} cm^3 $molecules^{-1}$ s^{-1} for $RO_2 + OH$, 0.01 s^{-1} for RO_2 isomerization, and 1.0×10^{-13} cm^3 $molecules^{-1}$ s^{-1} for primary $RO_2 + RO_2$ reactions for all our experiments (Ziemann and Atkinson, 2012; Yan et al., 2016; Praske et al., 2018; Orlando and Tyndall, 2012).

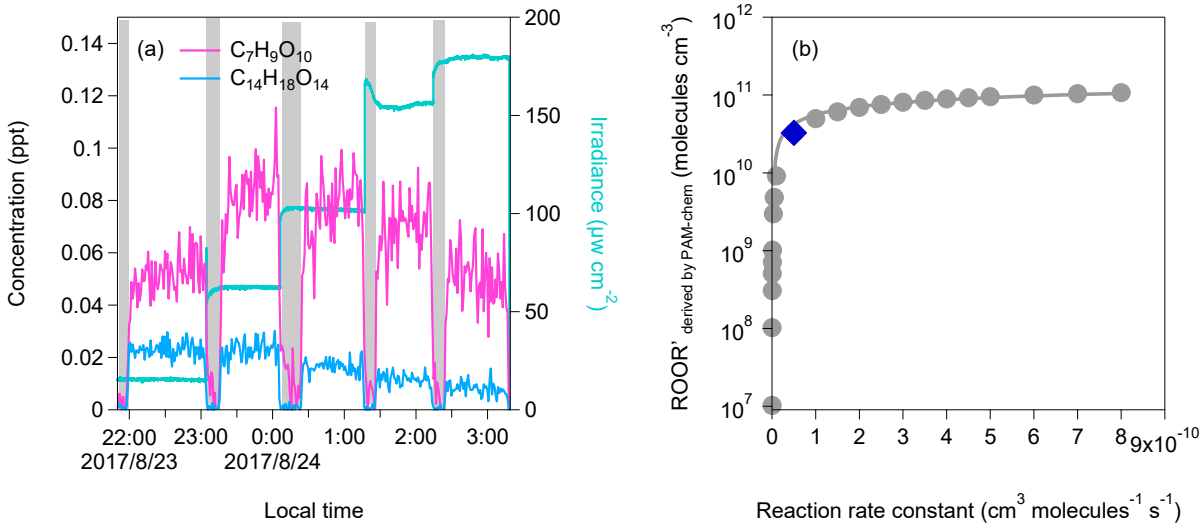

Figure S2. (a) Time series of experimental conditions (irradiance in the OFR) and the example monomeric and dimeric products from toluene oxidation. The grey shaded area represents "background" periods without VOC injection. **(b)** The simulated ROOR´ concentration under different reaction rate constant by using PAMchem model.

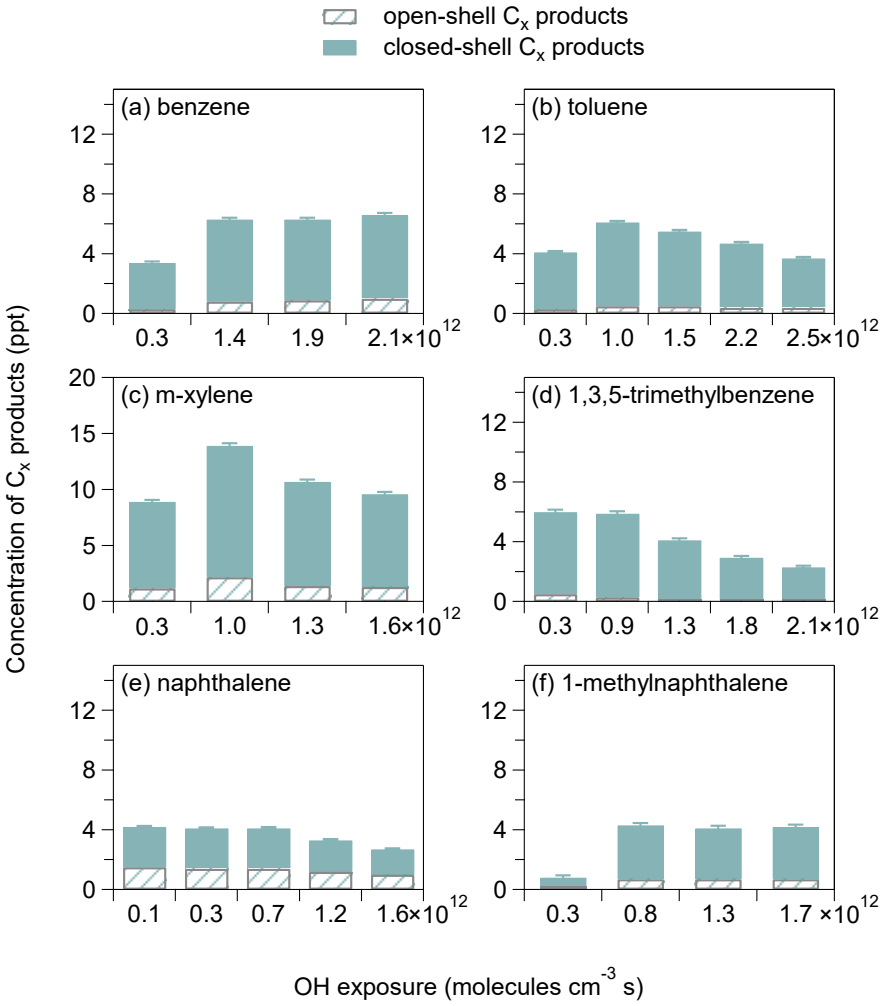

Figure S3. Concentrations of C_x products formed from the oxidation of **(a)** benzene, **(b)** toluene, **(c)** m-xylene, **(d)** 1,3,5-trimethylbenzene, **(e)** naphthalene and **(f)** 1-methylnaphthalene at different OH exposure. C_x products consist of open-shell and closed-shell monomers.

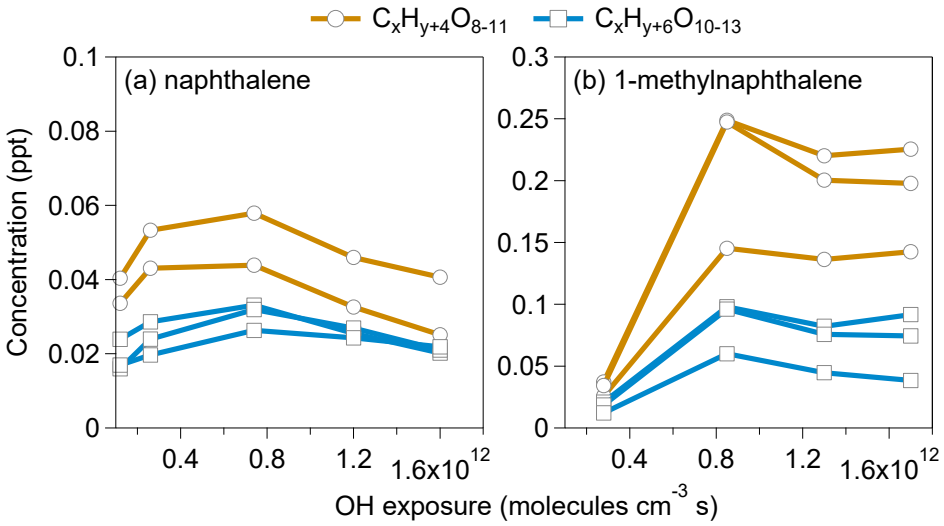

Figure S4. Concentrations of C_xH_{y+4}- and C_xH_{y+6}-series monomeric products formed from the oxidation of **(a)** naphthalene and **(b)** 1-methylnaphthalene at different OH exposure.

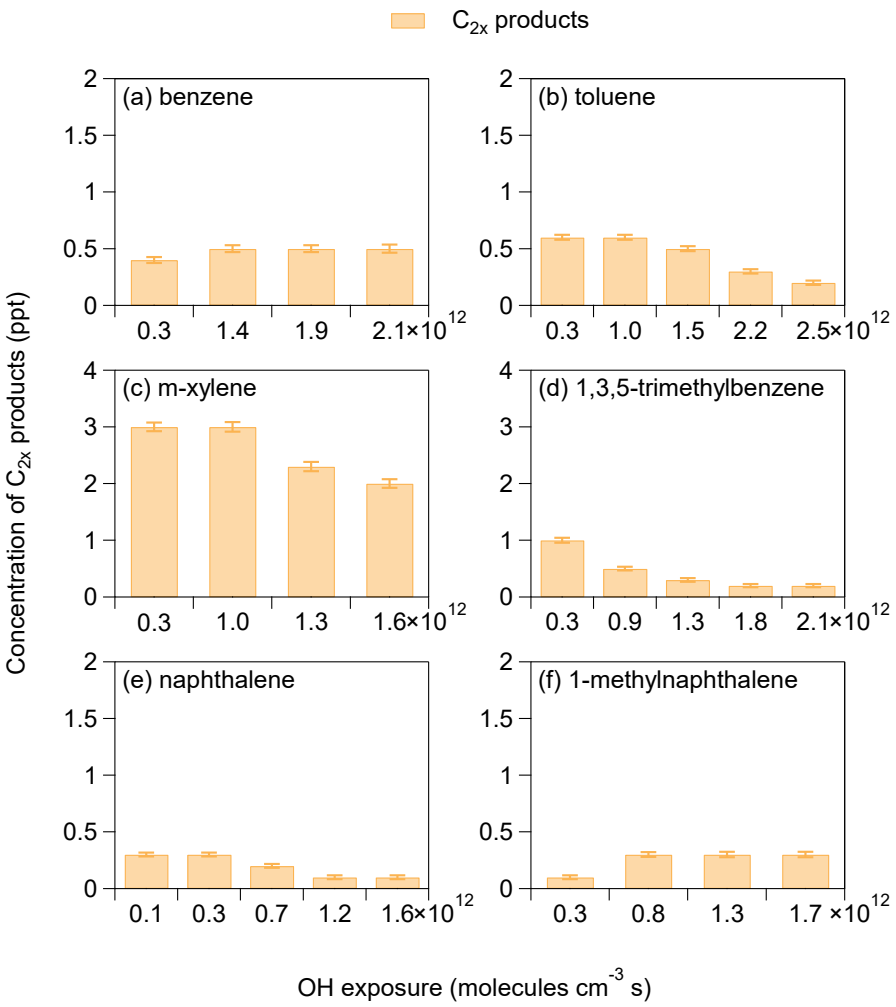

Figure S5. Concentrations of C_{2x} products formed from the oxidation of **(a)** benzene, **(b)** toluene, **(c)** m-xylene, **(d)** 1,3,5-trimethylbenzene, **(e)** naphthalene and **(f)** 1-methylnaphthalene at different OH exposure.

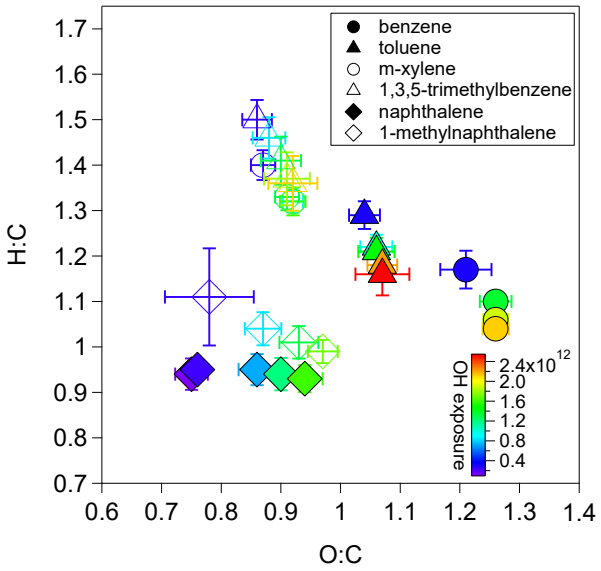

Figure S6. H:C and O:C ratios of gaseous OOMs formed from photooxidation of benzene, toluene, m-xylene, 1,3,5-trimethylbenzene, naphthalene and 1-methylnaphthalene at different OH exposure.

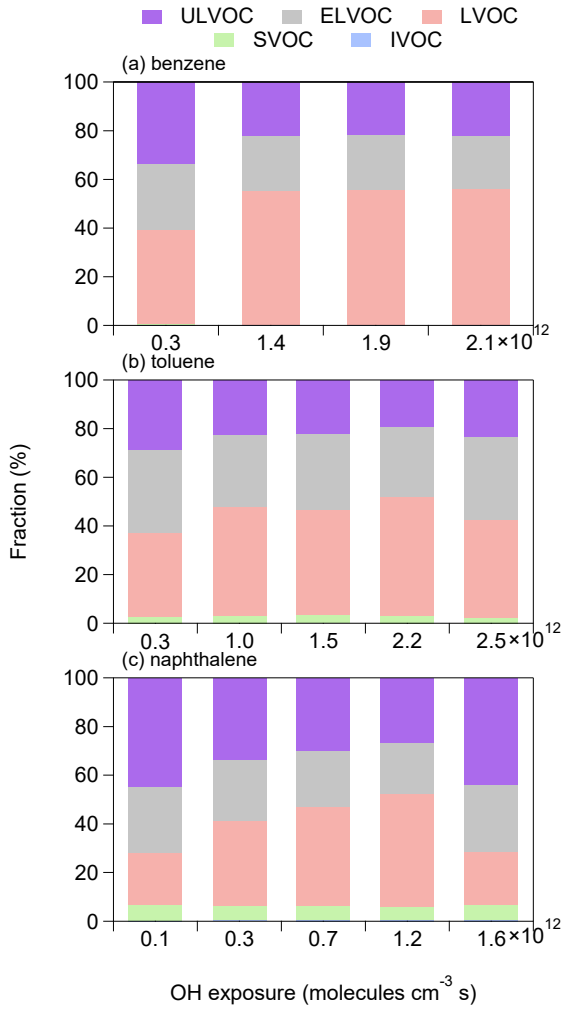

Figure S7. Concentration fractions of gaseous OOMs formed from the oxidation of **(a)** benzene, **(b)** toluene and **(c)** naphthalene at different OH exposure. OOMs are classified as five volatility classes: ULVOC, ELVOC, LVOC, SVOC, and IVOC. Volatilities of OOMs are calculated by using the method described in Wang et al. (2020).

Table S1. Yields of OOMs produced from photooxidation of benzene and toluene as a function of OH exposure in our OFR. The values difference is caused by the refitted spectra to up to 650 Th in this study.

VOC species	OH exposure (molec cm^{-3} s)	(Cheng et al., 2021)	This study
		Yield	Yield
benzene	3.1×10^{11}	0.06%	0.07%
	1.4×10^{12}	0.30%	0.31%
	1.9×10^{12}	0.26%	0.26%
	2.1×10^{12}	0.24%	0.24%
toluene	3.2×10^{11}	0.14%	0.17%
	9.8×10^{11}	0.65%	0.81%
	1.5×10^{12}	0.50%	0.61%
	2.2×10^{12}	0.59%	0.73%
	2.5×10^{12}	0.44%	0.46%

Table S2. Parts of the peak list for benzene (C_6H_6) oxidation products shown in Fig. 1a.

Category	Formula	*m/z* (Th)	Fraction of fitted signals
C_{2-5} monomeric products	$C_3H_4O_5$	181.99	9.2%
	$C_4H_4O_5$	193.99	14.3%
	$C_4H_6O_5$	196.01	2.1%
	$C_5H_4O_5$	205.99	6.6%
	$C_5H_6O_5$	208.01	1.5%
	$C_4H_4O_6$	209.99	2.6%
	$C_5H_4O_6$	221.99	7.8%
C_6 monomeric products	$C_6H_6O_5$	220.01	3.0%
	$C_6H_7O_5$	221.02	0.1%
	$C_6H_8O_5$	222.03	0.4%
	$C_6H_{10}O_5$	224.04	0.8%
	$C_6H_5O_6$	235.00	0.6%
	$C_6H_6O_6$	236.00	3.1%
	$C_6H_7O_6$	237.01	0.2%
	$C_6H_8O_6$	238.02	1.8%
	$C_6H_{10}O_6$	240.04	0.2%
	$C_6H_5O_7$	250.99	1.0%
	$C_6H_6O_7$	252.00	2.9%
	$C_6H_7O_7$	253.01	0.4%
	$C_6H_8O_7$	254.02	2.4%
	$C_6H_9O_7$	255.02	0.1%
	$C_6H_{10}O_7$	256.03	0.5%
	$C_6H_5O_8$	266.99	0.3%
	$C_6H_6O_8$	267.99	1.3%
	$C_6H_7O_8$	269.00	0.2%
	$C_6H_8O_8$	270.01	1.9%
	$C_6H_9O_8$	271.02	0.1%
	$C_6H_{10}O_8$	272.03	0.9%
	$C_6H_5O_9$	282.98	0.3%
	$C_6H_6O_9$	283.99	0.6%
	$C_6H_7O_9$	285.00	0.9%
	$C_6H_8O_9$	286.01	1.1%
	$C_6H_9O_9$	287.01	0.3%
	$C_6H_{10}O_9$	288.02	0.4%
	$C_6H_5O_{10}$	298.98	0.1%
	$C_6H_6O_{10}$	299.98	0.3%
	$C_6H_7O_{10}$	300.99	0.6%
	$C_6H_8O_{10}$	302.00	0.5%
	$C_6H_{10}O_{10}$	304.02	0.2%
C_{10-11} dimeric products	$C_{11}H_{14}O_9$	352.05	0.04%
	$C_{10}H_{10}O_{12}$	384.01	0.1%
	$C_{10}H_{12}O_{12}$	386.02	0.04%
C_{12} dimeric products	$C_{12}H_{14}O_8$	348.06	0.05%
	$C_{12}H_{14}O_9$	364.05	0.07%
	$C_{12}H_{10}O_{10}$	376.02	0.13%
	$C_{12}H_{12}O_{10}$	378.03	0.13%
	$C_{12}H_{14}O_{10}$	380.05	0.13%
	$C_{12}H_{16}O_{10}$	382.06	0.06%
	$C_{12}H_{10}O_{11}$	392.01	0.05%
	$C_{12}H_{12}O_{11}$	394.03	0.11%
	$C_{12}H_{14}O_{11}$	396.04	0.16%
	$C_{12}H_{16}O_{11}$	398.06	0.10%
	$C_{12}H_{10}O_{12}$	408.01	0.15%
	$C_{12}H_{12}O_{12}$	410.02	0.14%
	$C_{12}H_{14}O_{12}$	412.04	0.15%
	$C_{12}H_{16}O_{12}$	414.05	0.09%
	$C_{12}H_{10}O_{13}$	424.00	0.05%
	$C_{12}H_{12}O_{13}$	426.02	0.17%
	$C_{12}H_{14}O_{13}$	428.03	0.15%
	$C_{12}H_{16}O_{13}$	430.05	0.09%

$C_{12}H_{10}O_{14}$	440.00	0.06%
$C_{12}H_{12}O_{14}$	442.01	0.06%
$C_{12}H_{14}O_{14}$	444.03	0.1%
$C_{12}H_{16}O_{14}$	446.04	0.05%

Table S3. Parts of the peak list for toluene (C_7H_8) oxidation products shown in Fig. 1b.

Category	Formula	*m/z* (Th)	Fraction of total fitted signals
C_{2-6} monomeric products	$C_3H_4O_5$	181.99	2.4%
	$C_4H_4O_5$	193.99	5.9%
	$C_4H_6O_5$	196.01	9.5%
	$C_5H_4O_5$	205.99	3.5%
	$C_5H_6O_5$	208.01	5.7%
	$C_5H_4O_6$	221.99	7.2%
C_7 monomeric products	$C_7H_8O_5$	234.03	1.3%
	$C_7H_9O_5$	235.03	0.1%
	$C_7H_{10}O_5$	236.04	0.6%
	$C_7H_7O_6$	249.01	0.2%
	$C_7H_8O_6$	250.02	3.8%
	$C_7H_9O_6$	251.03	0.2%
	$C_7H_{10}O_6$	252.04	2.1%
	$C_7H_{12}O_6$	254.05	0.1%
	$C_7H_7O_7$	265.01	0.2%
	$C_7H_8O_7$	266.02	2.6%
	$C_7H_9O_7$	267.02	0.5%
	$C_7H_{10}O_7$	268.03	3.0%
	$C_7H_{11}O_7$	269.04	0.1%
	$C_7H_{12}O_7$	270.05	0.7%
	$C_7H_7O_8$	281.00	0.2%
	$C_7H_8O_8$	282.01	1.6%
	$C_7H_9O_8$	283.02	0.1%
	$C_7H_{10}O_8$	284.03	2.0%
	$C_7H_{11}O_8$	285.03	0.2%
	$C_7H_{12}O_8$	286.04	1.0%
	$C_7H_8O_9$	298.01	0.4%
	$C_7H_9O_9$	299.01	1.0%
	$C_7H_{10}O_9$	300.02	1.3%
	$C_7H_{11}O_9$	301.03	0.2%
	$C_7H_{12}O_9$	302.04	0.4%
	$C_7H_8O_{10}$	314.00	0.3%
	$C_7H_9O_{10}$	315.01	0.4%
	$C_7H_{10}O_{10}$	316.02	0.4%
	$C_7H_{12}O_{10}$	318.03	0.2%
C_{10-13} dimeric products	$C_{10}H_{10}O_9$	336.02	0.1%
	$C_{12}H_{10}O_8$	344.03	0.03%
	$C_{13}H_{12}O_9$	374.04	0.02%
	$C_{13}H_{14}O_{10}$	392.05	0.03%
C_{14} dimeric products	$C_{14}H_{18}O_8$	376.09	0.03%
	$C_{14}H_{16}O_9$	390.07	0.04%
	$C_{14}H_{18}O_9$	392.08	0.03%
	$C_{14}H_{20}O_9$	394.10	0.01%
	$C_{14}H_{16}O_{10}$	406.06	0.06%
	$C_{14}H_{18}O_{10}$	408.08	0.1%
	$C_{14}H_{20}O_{10}$	410.09	0.04%
	$C_{14}H_{16}O_{11}$	422.06	0.08%
	$C_{14}H_{18}O_{11}$	424.07	0.08%
	$C_{14}H_{20}O_{11}$	426.09	0.11%
	$C_{14}H_{16}O_{12}$	438.05	0.07%
	$C_{14}H_{18}O_{12}$	440.07	0.13%
	$C_{14}H_{20}O_{12}$	442.08	0.07%
	$C_{14}H_{16}O_{13}$	454.05	0.07%
	$C_{14}H_{18}O_{13}$	456.06	0.1%
	$C_{14}H_{20}O_{13}$	458.08	0.08%
	$C_{14}H_{16}O_{14}$	470.04	0.05%
	$C_{14}H_{18}O_{14}$	472.06	0.07%
	$C_{14}H_{20}O_{14}$	474.07	0.05%

Table S4. Parts of the peak list for m-xylene (C_8H_{10}) oxidation products shown in Fig. 1c.

Category	Formula	*m/z* (Th)	Fraction of total fitted signals
$C_{2\text{-}7}$ monomeric products	$C_3H_4O_5$	181.99	0.4%
	$C_4H_4O_5$	193.99	0.7%
	$C_5H_4O_5$	205.99	0.2%
	$C_5H_6O_5$	208.01	1.5%
	$C_4H_4O_6$	209.99	0.3%
	$C_5H_8O_5$	210.03	0.1%
	$C_4H_6O_6$	212.00	0.3%
	$C_5H_6O_6$	224.00	2.5%
C_8 monomeric products	$C_8H_{10}O_5$	248.04	0.06%
	$C_8H_{11}O_5$	249.05	0.05%
	$C_8H_{12}O_5$	250.06	0.2%
	$C_8H_8O_6$	262.02	0.5%
	$C_8H_{10}O_6$	264.04	2.3%
	$C_8H_{11}O_6$	265.04	0.7%
	$C_8H_{12}O_6$	266.05	1.5%
	$C_8H_{13}O_6$	267.06	0.1%
	$C_8H_{14}O_6$	268.07	0.2%
	$C_8H_8O_7$	278.02	1.6%
	$C_8H_9O_7$	279.02	0.1%
	$C_8H_{10}O_7$	280.03	8.6%
	$C_8H_{11}O_7$	281.04	0.9%
	$C_8H_{12}O_7$	282.05	4.4%
	$C_8H_{13}O_7$	283.05	0.4%
	$C_8H_{14}O_7$	284.06	1.8%
	$C_8H_8O_8$	294.01	0.6%
	$C_8H_9O_8$	295.02	0.1%
	$C_8H_{10}O_8$	296.03	6.4%
	$C_8H_{11}O_8$	297.03	0.9%
	$C_8H_{12}O_8$	298.04	4.6%
	$C_8H_{13}O_8$	299.05	0.9%
	$C_8H_{14}O_8$	300.06	3.5%
	$C_8H_{10}O_9$	312.02	2.6%
	$C_8H_{11}O_9$	313.03	1.0%
	$C_8H_{12}O_9$	314.04	4.4%
	$C_8H_{13}O_9$	315.04	0.6%
	$C_8H_{14}O_9$	316.05	2.3%
	$C_8H_9O_{10}$	327.01	0.1%
	$C_8H_{10}O_{10}$	328.02	0.5%
	$C_8H_{11}O_{10}$	329.02	0.1%
	$C_8H_{12}O_{10}$	330.03	1.0%
	$C_8H_{13}O_{10}$	331.04	0.5%
	$C_8H_{14}O_{10}$	332.05	0.6%
$C_{10\text{-}15}$ dimeric products	$C_{14}H_8O_5$	318.03	0.14%
	$C_{13}H_{10}O_6$	324.04	0.11%
	$C_{11}H_{14}O_8$	336.06	0.07%
	$C_{14}H_{12}O_6$	338.05	0.16%
	$C_{13}H_{10}O_8$	356.03	0.06%
	$C_{14}H_{20}O_{10}$	410.09	0.18%
C_{16} dimeric products	$C_{16}H_{18}O_7$	384.09	0.11%
	$C_{16}H_{18}O_8$	400.09	0.1%
	$C_{16}H_{18}O_9$	416.08	0.08%
	$C_{16}H_{20}O_9$	418.10	0.06%
	$C_{16}H_{22}O_9$	420.11	0.11%
	$C_{16}H_{18}O_{10}$	432.08	0.08%
	$C_{16}H_{20}O_{10}$	434.09	0.14%
	$C_{16}H_{22}O_{10}$	436.11	0.3%
	$C_{16}H_{24}O_{10}$	438.13	0.28%
	$C_{16}H_{20}O_{11}$	450.09	0.26%
	$C_{16}H_{22}O_{11}$	452.10	0.37%
	$C_{16}H_{24}O_{11}$	454.12	0.48%

$C_{16}H_{20}O_{12}$	466.08	0.33%
$C_{16}H_{22}O_{12}$	468.10	0.54%
$C_{16}H_{24}O_{12}$	470.12	0.47%
$C_{16}H_{20}O_{13}$	482.08	0.3%
$C_{16}H_{22}O_{13}$	484.09	0.46%
$C_{16}H_{24}O_{13}$	486.11	0.47%
$C_{16}H_{20}O_{14}$	498.07	0.19%
$C_{16}H_{22}O_{14}$	500.09	0.32%
$C_{16}H_{24}O_{14}$	502.10	0.27%

Table S5. Parts of the peak list for 1,3,5-trimethylbenzene (C_9H_{12}) oxidation products shown in Fig. 1d.

Category	Formula	*m/z* (Th)	Fraction of total fitted signals
$C_{2\text{-}8}$ monomeric products	$C_3H_4O_5$	181.99	0.2%
	$C_4H_4O_5$	193.99	0.7%
	$C_5H_4O_5$	205.99	0.1%
	$C_5H_6O_5$	208.01	0.6%
	$C_4H_4O_6$	209.99	0.3%
	$C_5H_8O_5$	210.03	0.1%
	$C_4H_6O_6$	212.00	0.5%
	$C_6H_6O_5$	220.01	0.3%
	$C_5H_4O_6$	221.99	0.5%
	$C_5H_6O_6$	224.00	0.8%
	$C_6H_6O_6$	236.00	0.9%
	$C_6H_8O_6$	238.02	0.9%
	$C_7H_{10}O_6$	252.04	0.8%
	$C_8H_{10}O_6$	264.04	1.5%
	$C_7H_8O_7$	266.02	0.7%
	$C_8H_{10}O_7$	280.03	3.1%
	$C_8H_{12}O_7$	282.05	1.8%
C_9 monomeric products	$C_9H_{12}O_5$	262.06	0.2%
	$C_9H_{13}O_5$	263.06	0.1%
	$C_9H_{12}O_6$	278.05	2.7%
	$C_9H_{14}O_6$	280.07	1.4%
	$C_9H_{16}O_6$	282.08	0.2%
	$C_9H_{10}O_7$	292.03	0.7%
	$C_9H_{12}O_7$	294.05	4.4%
	$C_9H_{13}O_7$	295.05	0.13%
	$C_9H_{14}O_7$	296.06	17.5%
	$C_9H_{15}O_7$	297.07	1.6%
	$C_9H_{16}O_7$	298.08	3.4%
	$C_9H_{10}O_8$	308.03	0.5%
	$C_9H_{12}O_8$	310.04	6.0%
	$C_9H_{13}O_8$	311.05	0.3%
	$C_9H_{14}O_8$	312.06	4.3%
	$C_9H_{15}O_8$	313.07	0.5%
	$C_9H_{16}O_8$	314.07	3.7%
	$C_9H_{10}O_9$	324.02	0.6%
	$C_9H_{12}O_9$	326.04	2.3%
	$C_9H_{13}O_9$	327.04	0.4%
	$C_9H_{14}O_9$	328.05	4.1%
	$C_9H_{15}O_9$	329.06	0.4%
	$C_9H_{16}O_9$	330.07	2.8%
	$C_9H_{10}O_{10}$	340.02	0.1%
	$C_9H_{12}O_{10}$	342.03	0.9%
	$C_9H_{13}O_{10}$	343.04	0.7%
	$C_9H_{14}O_{10}$	344.05	1.4%
	$C_9H_{15}O_{10}$	345.05	0.5%
	$C_9H_{16}O_{10}$	346.06	0.8%
$C_{10\text{-}17}$ dimeric products	$C_{11}H_{18}O_8$	340.09	0.09%
	$C_{12}H_{18}O_8$	352.09	0.13%
	$C_{11}H_{16}O_9$	354.07	0.05%
	$C_{14}H_{14}O_7$	356.06	0.05%
	$C_{12}H_{10}O_{12}$	408.01	0.12%
C_{18} dimeric products	$C_{18}H_{24}O_{10}$	462.13	0.09%
	$C_{18}H_{26}O_{10}$	464.14	0.19%
	$C_{18}H_{28}O_{10}$	466.16	0.08%
	$C_{18}H_{24}O_{11}$	478.12	0.11%
	$C_{18}H_{26}O_{11}$	480.14	0.13%
	$C_{18}H_{28}O_{11}$	482.15	0.16%
	$C_{18}H_{24}O_{12}$	494.12	0.23%
	$C_{18}H_{26}O_{12}$	496.13	0.37%
	$C_{18}H_{28}O_{12}$	498.15	0.22%

$C_{18}H_{24}O_{13}$	510.11	0.1%
$C_{18}H_{26}O_{13}$	512.13	0.23%
$C_{18}H_{28}O_{13}$	514.14	0.18%
$C_{18}H_{24}O_{14}$	526.10	0.12%
$C_{18}H_{26}O_{14}$	528.12	0.18%
$C_{18}H_{28}O_{14}$	530.14	0.17%

Table S6. Parts of the peak list for naphthalene ($C_{10}H_8$) oxidation products shown in Fig. 1e.

Category	Formula	*m/z* (Th)	Fraction of total fitted signals
$C_{2\text{-}9}$ monomeric products	$C_3H_4O_5$	181.99	8.9%
	$C_4H_4O_5$	193.99	9.3%
	$C_4H_6O_5$	196.01	1.7%
	$C_5H_4O_5$	205.99	3.7%
	$C_5H_6O_5$	208.01	1.0%
	$C_4H_4O_6$	209.99	2.3%
	$C_6H_6O_5$	220.01	1.0%
	$C_5H_4O_6$	221.99	2.5%
	$C_5H_8O_6$	226.02	5.6%
	$C_7H_6O_6$	248.00	0.6%
	$C_9H_8O_7$	290.02	2.1%
C_{10} monomeric products	$C_{10}H_6O_5$	268.01	0.6%
	$C_{10}H_7O_5$	269.02	0.2%
	$C_{10}H_8O_5$	270.03	2.8%
	$C_{10}H_9O_5$	271.03	0.4%
	$C_{10}H_{10}O_5$	272.04	0.5%
	$C_{10}H_{11}O_5$	273.05	0.1%
	$C_{10}H_{12}O_5$	274.06	0.2%
	$C_{10}H_{13}O_5$	275.06	0.1%
	$C_{10}H_6O_6$	284.00	0.5%
	$C_{10}H_7O_6$	285.01	0.1%
	$C_{10}H_8O_6$	286.02	2.9%
	$C_{10}H_9O_6$	287.03	0.3%
	$C_{10}H_{10}O_6$	288.04	0.9%
	$C_{10}H_{11}O_6$	289.04	0.5%
	$C_{10}H_{12}O_6$	290.05	0.3%
	$C_{10}H_{13}O_6$	291.06	0.2%
	$C_{10}H_{14}O_6$	292.07	0.1%
	$C_{10}H_6O_7$	300.00	0.1%
	$C_{10}H_7O_7$	301.01	0.3%
	$C_{10}H_8O_7$	302.02	1.8%
	$C_{10}H_9O_7$	303.02	1.0%
	$C_{10}H_{10}O_7$	304.03	1.0%
	$C_{10}H_{11}O_7$	305.04	0.3%
	$C_{10}H_{12}O_7$	306.05	0.2%
	$C_{10}H_{13}O_7$	307.05	0.1%
	$C_{10}H_{14}O_7$	308.06	0.1%
	$C_{10}H_6O_8$	315.99	0.1%
	$C_{10}H_7O_8$	317.00	0.3%
	$C_{10}H_8O_8$	318.01	0.5%
	$C_{10}H_9O_8$	319.02	1.1%
	$C_{10}H_{10}O_8$	320.03	1.0%
	$C_{10}H_{11}O_8$	321.03	0.3%
	$C_{10}H_{12}O_8$	322.04	0.3%
	$C_{10}H_{13}O_8$	323.05	0.1%
	$C_{10}H_{14}O_8$	324.06	0.1%
	$C_{10}H_6O_9$	331.99	0.1%
	$C_{10}H_7O_9$	333.00	0.1%
	$C_{10}H_8O_9$	334.01	0.4%
	$C_{10}H_9O_9$	335.01	0.3%
	$C_{10}H_{10}O_9$	336.02	0.6%
	$C_{10}H_{11}O_9$	337.03	0.3%
	$C_{10}H_{12}O_9$	338.04	0.5%
	$C_{10}H_{13}O_9$	339.04	0.1%
	$C_{10}H_{14}O_9$	340.05	0.1%
	$C_{10}H_7O_{10}$	348.99	0.4%
	$C_{10}H_8O_{10}$	350.00	0.2%
	$C_{10}H_9O_{10}$	351.01	0.5%
	$C_{10}H_{10}O_{10}$	352.02	0.7%
	$C_{10}H_{11}O_{10}$	353.02	0.4%
	$C_{10}H_{12}O_{10}$	354.03	0.6%

	$C_{10}H_7O_{11}$	364.99	0.2%
	$C_{10}H_8O_{11}$	366.00	0.2%
	$C_{10}H_9O_{11}$	367.00	0.2%
	$C_{10}H_{10}O_{11}$	368.01	0.4%
	$C_{10}H_{11}O_{11}$	369.02	0.2%
	$C_{10}H_{12}O_{11}$	370.03	0.6%
	$C_{10}H_{13}O_{11}$	371.03	0.2%
	$C_{10}H_{14}O_{11}$	372.04	0.3%
	$C_{10}H_7O_{12}$	380.98	0.1%
	$C_{10}H_8O_{12}$	381.99	0.1%
	$C_{10}H_9O_{12}$	383.00	0.1%
	$C_{10}H_{10}O_{12}$	384.01	0.2%
	$C_{10}H_{11}O_{12}$	385.01	0.2%
	$C_{10}H_{12}O_{12}$	386.02	0.4%
	$C_{10}H_{13}O_{12}$	387.03	0.1%
	$C_{10}H_{14}O_{12}$	388.04	0.2%
	$C_{11}H_{14}O_{13}$	416.03	0.02%
$C_{11\text{-}19}$ dimeric products	$C_{14}H_{14}O_{12}$	436.04	0.04%
	$C_{18}H_{12}O_{12}$	482.02	0.02%
	$C_{20}H_{14}O_8$	444.06	0.01%
	$C_{20}H_{16}O_8$	446.07	0.02%
	$C_{20}H_{16}O_9$	462.07	0.03%
	$C_{20}H_{18}O_9$	464.08	0.01%
	$C_{20}H_{14}O_{10}$	476.05	0.02%
	$C_{20}H_{16}O_{10}$	478.06	0.03%
	$C_{20}H_{18}O_{10}$	480.08	0.02%
	$C_{20}H_{14}O_{11}$	492.04	0.02%
	$C_{20}H_{16}O_{11}$	494.06	0.03%
C_{20} dimeric products	$C_{20}H_{18}O_{11}$	496.07	0.03%
	$C_{20}H_{20}O_{11}$	498.09	0.02%
	$C_{20}H_{14}O_{12}$	508.04	0.02%
	$C_{20}H_{16}O_{12}$	510.05	0.01%
	$C_{20}H_{18}O_{12}$	512.07	0.02%
	$C_{20}H_{20}O_{12}$	514.08	0.03%
	$C_{20}H_{22}O_{12}$	516.10	0.01%
	$C_{20}H_{20}O_{13}$	530.08	0.01%
	$C_{20}H_{18}O_{14}$	544.06	0.02%
	$C_{20}H_{20}O_{14}$	546.07	0.03%

Table S7. Parts of the peak list for 1-methylnaphthalene ($C_{11}H_{10}$) oxidation products shown in Fig. 1f.

Category	Formula	*m/z* (Th)	Fraction of total fitted signals
$C_{2\text{-}10}$ monomeric products	$C_3H_4O_5$	181.99	4.1%
	$C_4H_4O_5$	193.99	2.7%
	$C_4H_6O_5$	196.01	0.4%
	$C_5H_4O_5$	205.99	0.8%
	$C_5H_6O_5$	208.01	1.0%
	$C_4H_6O_6$	212.00	0.6%
	$C_5H_4O_6$	221.99	4.0%
	$C_5H_6O_6$	224.00	3.0%
	$C_6H_6O_6$	236.00	1.9%
	$C_5H_6O_7$	240.00	1.2%
	$C_6H_6O_7$	252.00	2.8%
C_{11} monomeric products	$C_{11}H_{10}O_5$	284.04	0.4%
	$C_{11}H_{11}O_5$	285.05	0.05
	$C_{11}H_{12}O_5$	286.06	0.1%
	$C_{11}H_8O_6$	298.02	0.7%
	$C_{11}H_9O_6$	299.03	0.1%
	$C_{11}H_{10}O_6$	300.04	0.7%
	$C_{11}H_{11}O_6$	301.04	0.1%
	$C_{11}H_{12}O_6$	302.05	0.2%
	$C_{11}H_8O_7$	314.02	0.4%
	$C_{11}H_9O_7$	315.02	0.2%
	$C_{11}H_{10}O_7$	316.03	0.6%
	$C_{11}H_{11}O_7$	317.04	0.1%
	$C_{11}H_{12}O_7$	318.05	0.4%
	$C_{11}H_{14}O_7$	320.06	0.2%
	$C_{11}H_8O_8$	330.01	0.4%
	$C_{11}H_9O_8$	331.02	0.1%
	$C_{11}H_{10}O_8$	332.03	0.8%
	$C_{11}H_{11}O_8$	333.03	0.2%
	$C_{11}H_{12}O_8$	334.04	1.0%
	$C_{11}H_{13}O_8$	335.05	0.1%
	$C_{11}H_{14}O_8$	336.06	0.5%
	$C_{11}H_8O_9$	346.01	0.3%
	$C_{11}H_9O_9$	347.01	0.1%
	$C_{11}H_{10}O_9$	348.02	0.9%
	$C_{11}H_{11}O_9$	349.03	0.1%
	$C_{11}H_{12}O_9$	350.04	1.6%
	$C_{11}H_{13}O_9$	351.04	0.2%
	$C_{11}H_{14}O_9$	352.05	1.1%
	$C_{11}H_{16}O_9$	354.07	0.2%
	$C_{11}H_8O_{10}$	362.00	0.4%
	$C_{11}H_9O_{10}$	363.01	0.2%
	$C_{11}H_{10}O_{10}$	364.02	1.0%
	$C_{11}H_{11}O_{10}$	365.02	0.1%
	$C_{11}H_{12}O_{10}$	366.03	2.1%
	$C_{11}H_{13}O_{10}$	367.04	0.2%
	$C_{11}H_{14}O_{10}$	368.05	1.9%
	$C_{11}H_{16}O_{10}$	370.06	0.5%
	$C_{11}H_{10}O_{11}$	380.01	0.8%
	$C_{11}H_{11}O_{11}$	381.02	0.1%
	$C_{11}H_{12}O_{11}$	382.03	1.8%
	$C_{11}H_{13}O_{11}$	383.03	0.2%
	$C_{11}H_{14}O_{11}$	384.04	1.8%
	$C_{11}H_{16}O_{11}$	386.06	0.7%
	$C_{11}H_{10}O_{12}$	396.01	0.4%
	$C_{11}H_{11}O_{12}$	397.01	0.2%
	$C_{11}H_{12}O_{12}$	398.02	1.3%
	$C_{11}H_{13}O_{12}$	399.03	0.2%
	$C_{11}H_{14}O_{12}$	400.04	1.3%
	$C_{11}H_{16}O_{12}$	402.05	0.6%
	$C_{11}H_{10}O_{13}$	412.00	0.2%

	$C_{11}H_{11}O_{13}$	413.01	0.1%
	$C_{11}H_{12}O_{13}$	414.02	0.6%
	$C_{11}H_{13}O_{13}$	415.02	0.2%
	$C_{11}H_{14}O_{13}$	416.03	0.7%
	$C_{11}H_{16}O_{13}$	418.05	0.4%
	$C_{11}H_{10}O_{14}$	428.00	0.1%
	$C_{11}H_{12}O_{14}$	430.01	0.3%
	$C_{11}H_{13}O_{14}$	431.02	0.1%
	$C_{11}H_{14}O_{14}$	432.03	0.4%
	$C_{11}H_{16}O_{14}$	434.04	0.2%
C_{12-21} dimeric products	$C_{13}H_{18}O_4$	300.11	0.04%
	$C_{20}H_{10}O_5$	392.04	0.02%
C_{22} dimeric products	$C_{22}H_{18}O_9$	488.08	0.02%
	$C_{22}H_{22}O_9$	492.11	0.02%
	$C_{22}H_{18}O_{10}$	504.08	0.02%
	$C_{22}H_{20}O_{10}$	506.09	0.02%
	$C_{22}H_{22}O_{10}$	508.11	0.02%
	$C_{22}H_{24}O_{10}$	510.13	0.02%
	$C_{22}H_{18}O_{11}$	520.07	0.04%
	$C_{22}H_{20}O_{11}$	522.09	0.03%
	$C_{22}H_{22}O_{11}$	524.10	0.04%
	$C_{22}H_{24}O_{11}$	526.12	0.02%
	$C_{22}H_{20}O_{12}$	538.08	0.04%
	$C_{22}H_{22}O_{12}$	540.10	0.05%
	$C_{22}H_{24}O_{12}$	542.12	0.04%
	$C_{22}H_{18}O_{13}$	552.06	0.03%
	$C_{22}H_{20}O_{13}$	554.08	0.03%
	$C_{22}H_{22}O_{13}$	556.09	0.04%
	$C_{22}H_{24}O_{13}$	558.11	0.04%
	$C_{22}H_{18}O_{14}$	568.06	0.01%
	$C_{22}H_{20}O_{14}$	570.07	0.06%
	$C_{22}H_{22}O_{14}$	572.09	0.05%
	$C_{22}H_{24}O_{14}$	574.10	0.04%

Table S8. Fraction of the major C_x-series monomers, and C_{2x}-series dimers selected from Tables S2-S7.

	benzene (%)	toluene (%)	m-xylene (%)	1,3,5-trimethylbenzene (%)	naphthalene (%)	1-methylnaphthalene (%)
$C_xH_{y+1}O_5$	0.1	0.1	0.05	0.1	0.4	0.05
$C_xH_{y+1}O_6$	0.2	0.2	0.7	/	0.3	0.1
$C_xH_{y+1}O_7$	0.4	0.5	0.9	0.13	1	0.1
$C_xH_{y+1}O_8$	0.2	0.1	0.9	0.3	1.1	0.2
$C_xH_{y+1}O_9$	0.9	1	1	0.4	0.3	0.1
$C_{2x}H_{2y}O_{10-14}$	0.6	0.3	1.2	0.7	0.1	0.2
$C_{2x}H_{2y+2}O_{10-14}$	0.7	0.5	2.0	1.1	0.1	0.2
$C_{2x}H_{2y+4}O_{10-14}$	0.4	0.4	2.0	0.8	0.1	0.2

References

Bianchi, F., Kurten, T., Riva, M., Mohr, C., Rissanen, M. P., Roldin, P., Berndt, T., Crounse, J. D., Wennberg, P. O., Mentel, T. F., Wildt, J., Junninen, H., Jokinen, T., Kulmala, M., Worsnop, D. R., Thornton, J. A., Donahue, N., Kjaergaard, H. G., and Ehn, M.: Highly oxygenated organic molecules (HOM) from gas-phase autoxidation involving peroxy radicals: a key contributor to atmospheric aerosol, Chem. Rev., 119, 3472-3509, https://doi.org/10.1021/acs.chemrev.8b00395, 2019.

Brune, W. H.: The chamber wall index for gas-wall interactions in atmospheric environmental enclosures, Environ. Sci. Technol., 53, 3645-3652, https://doi.org/10.1021/acs.est.8b06260, 2019.

Cheng, X., Chen, Q., Li, Y., Zheng, Y., Liao, K., and Huang, G.: Highly oxygenated organic molecules produced by the oxidation of benzene and toluene in a wide range of OH exposure and NOx conditions, Atmos. Chem. Phys., 21, 12005-12019, https://doi.org/10.5194/acp-21-12005-2021, 2021.

Donahue, N. M., Epstein, S. A., Pandis, S. N., and Robinson, A. L.: A two-dimensional volatility basis set: 1. organic-aerosol mixing thermodynamics, Atmos. Chem. Phys., 11, 3303-3318, https://doi.org/10.5194/acp-11-3303-2011, 2011.

Donahue, N. M., Robinson, A. L., Stanier, C. O., and Pandis, S. N.: Coupled partitioning, dilution, and chemical aging of semivolatile organics, Environ. Sci. Technol., 40, 2635-2643, https://doi.org/10.1021/es052297c, 2006.

Epstein, S. A., Riipinen, I., and Donahue, N. M.: A Semiempirical Correlation between Enthalpy of Vaporization and Saturation Concentration for Organic Aerosol, Environ. Sci. Technol., 44, 743-748, https://doi.org/10.1021/es902497z, 2010.

Fuller, E. N., Schettler, P. D., and Giddings, J. C.: A new method for prediction of binary gas-phase diffusion coefficients, Ind. Eng. Chem., 58, 18-27, https://doi.org/10.1021/ie50677a007, 1966.

Garmash, O., Rissanen, M. P., Pullinen, I., Schmitt, S., Kausiala, O., Tillmann, R., Zhao, D., Percival, C., Bannan, T. J., Priestley, M., Hallquist, Å. M., Kleist, E., Kiendler-Scharr, A., Hallquist, M., Berndt, T., McFiggans, G., Wildt, J., Mentel, T. F., and Ehn, M.: Multi-generation OH oxidation as a source for highly oxygenated organic molecules from aromatics, Atmos. Chem. Phys., 20, 515-537, https://doi.org/10.5194/acp-20-515-2020, 2020.

Huang, Y. L., Zhao, R., Charan, S. M., Kenseth, C. M., Zhang, X., and Seinfeld, J. H.: Unified theory of vapor-wall mass transport in teflon-walled environmental chambers, Environ. Sci. Technol., 52, 2134-2142, https://doi.org/10.1021/acs.est.7b05575, 2018.

Jenkin, M. E., Saunders, S. M., Wagner, V., and Pilling, M. J.: Protocol for the development of the Master Chemical Mechanism, MCM v3 (Part B): tropospheric degradation of aromatic volatile organic compounds, Atmos. Chem. Phys., 3, 181-193, https://doi.org/10.5194/acp-3-181-2003, 2003.

Kulmala, M., Petäjä, T., Nieminen, T., Sipilä, M., Manninen, H. E., Lehtipalo, K., Dal Maso, M., Aalto, P. P., Junninen, H., Paasonen, P., Riipinen, I., Lehtinen, K. E. J., Laaksonen, A., and Kerminen, V.-M.: Measurement of the nucleation of atmospheric aerosol particles, Nat. Protoc., 7, 1651-1667, https://doi.org/10.1038/nprot.2012.091, 2012.

Kulmala, M., Toivonen, A., Mäkelä, J. M., and Laaksonen, A.: Analysis of the growth of nucleation mode particles observed in boreal forest, Tellus B, 50, 449-462, https://doi.org/10.3402/tellusb.v50i5.16229, 1998.

McMurry, P. H., and Grosjean, D.: Gas and aerosol wall losses in Teflon film smog chambers, Environ. Sci. Technol., 19, 1176-1182, https://doi.org/10.1021/es00142a006, 1985.

Nishino, N., Arey, J., and Atkinson, R.: 2-Formylcinnamaldehyde formation yield from the OH radical-initiated reaction of naphthalene: effect of NO2 concentration, Environ. Sci. Technol., 46, 8198-8204, https://doi.org/10.1021/es301865t, 2012.

Orlando, J. J., and Tyndall, G. S.: Laboratory studies of organic peroxy radical chemistry: an overview with emphasis on recent issues of atmospheric significance, Chem. Soc. Rev., 41, 6294-6317, https://doi.org/10.1039/C2CS35166H, 2012.

Palm, B. B., Campuzano-Jost, P., Ortega, A. M., Day, D. A., Kaser, L., Jud, W., Karl, T., Hansel, A., Hunter, J. F., Cross, E.

S., Kroll, J. H., Peng, Z., Brune, W. H., and Jimenez, J. L.: In situ secondary organic aerosol formation from ambient pine forest air using an oxidation flow reactor, Atmos. Chem. Phys., 16, 2943-2970, https://doi.org/10.5194/acp-16-2943-2016, 2016.

Pankow, J. F.: An absorption model of gas/particle partitioning of organic compounds in the atmosphere, Atmos. Environ., 28, 185-188, https://doi.org/10.1016/1352-2310(94)90093-0, 1994.

Praske, E., Otkjær, R. V., Crounse, J. D., Hethcox, J. C., Stoltz, B. M., Kjaergaard, H. G., and Wennberg, P. O.: Atmospheric autoxidation is increasingly important in urban and suburban North America, Proc. Natl. Acad. Sci. U. S. A., 115, 64-69, https://doi.org/10.1073/pnas.1715540115, 2018.

Schervish, M., and Donahue, N. M.: Peroxy radical chemistry and the volatility basis set, Atmos. Chem. Phys., 20, 1183-1199, https://doi.org/10.5194/acp-20-1183-2020, 2020.

Shrivastava, M., Cappa, C. D., Fan, J., Goldstein, A. H., Guenther, A. B., Jimenez, J. L., Kuang, C., Laskin, A., Martin, S. T., Ng, N. L., Petaja, T., Pierce, J. R., Rasch, P. J., Roldin, P., Seinfeld, J. H., Shilling, J., Smith, J. N., Thornton, J. A., Volkamer, R., Wang, J., Worsnop, D. R., Zaveri, R. A., Zelenyuk, A., and Zhang, Q.: Recent advances in understanding secondary organic aerosol: implications for global climate forcing, Rev. Geophys., 55, 509-559, https://doi.org/10.1002/2016rg000540, 2017.

Tröstl, J., Chuang, W. K., Gordon, H., Heinritzi, M., Yan, C., Molteni, U., Ahlm, L., Frege, C., Bianchi, F., Wagner, R., Simon, M., Lehtipalo, K., Williamson, C., Craven, J. S., Duplissy, J., Adamov, A., Almeida, J., Bernhammer, A.-K., Breitenlechner, M., Brilke, S., Dias, A., Ehrhart, S., Flagan, R. C., Franchin, A., Fuchs, C., Guida, R., Gysel, M., Hansel, A., Hoyle, C. R., Jokinen, T., Junninen, H., Kangasluoma, J., Keskinen, H., Kim, J., Krapf, M., Kürten, A., Laaksonen, A., Lawler, M., Leiminger, M., Mathot, S., Möhler, O., Nieminen, T., Onnela, A., Petäjä, T., Piel, F. M., Miettinen, P., Rissanen, M. P., Rondo, L., Sarnela, N., Schobesberger, S., Sengupta, K., Sipilä, M., Smith, J. N., Steiner, G., Tomè, A., Virtanen, A., Wagner, A. C., Weingartner, E., Wimmer, D., Winkler, P. M., Ye, P., Carslaw, K. S., Curtius, J., Dommen, J., Kirkby, J., Kulmala, M., Riipinen, I., Worsnop, D. R., Donahue, N. M., and Baltensperger, U.: The role of low-volatility organic compounds in initial particle growth in the atmosphere, Nature, 533, 527-531, https://doi.org/10.1038/nature18271, 2016.

Wang, M., Chen, D., Xiao, M., Ye, Q., Stolzenburg, D., Hofbauer, V., Ye, P., Vogel, A. L., Mauldin, R. L., Amorim, A., Baccarini, A., Baumgartner, B., Brilke, S., Dada, L., Dias, A., Duplissy, J., Finkenzeller, H., Garmash, O., He, X.-C., Hoyle, C. R., Kim, C., Kvashnin, A., Lehtipalo, K., Fischer, L., Molteni, U., Petäjä, T., Pospisilova, V., Quéléver, L. L. J., Rissanen, M., Simon, M., Tauber, C., Tomé, A., Wagner, A. C., Weitz, L., Volkamer, R., Winkler, P. M., Kirkby, J., Worsnop, D. R., Kulmala, M., Baltensperger, U., Dommen, J., El-Haddad, I., and Donahue, N. M.: Photo-oxidation of aromatic hydrocarbons produces low-volatility organic compounds, Environ. Sci. Technol., 54, 7911-7921, https://doi.org/10.1021/acs.est.0c02100, 2020.

Yan, C., Kocevska, S., and Krasnoperov, L. N.: Kinetics of the reaction of CH3O2 radicals with OH studied over the 292-526 K temperature range, J. Phys. Chem. A, 120, 6111-6121, https://doi.org/10.1021/acs.jpca.6b04213, 2016.

Ziemann, P. J., and Atkinson, R.: Kinetics, products, and mechanisms of secondary organic aerosol formation, Chem. Soc. Rev., 41, 6582-6605, https://doi.org/10.1039/C2CS35122F, 2012.